Developmental Biology 502 (2023) 50–62

Contents lists available at ScienceDirect

Developmental Biology

journal homepage: www.elsevier.com/locate/developmentalbiology

microRNA-124 directly suppresses *Nodal* and *Notch* to regulate mesodermal development

Kalin D. Konrad [a,2], Malcolm Arnott [a,1], Michael Testa [a,1], Santiago Suarez [a,b], Jia L. Song [a,*]

[a] Department of Biological Sciences, University of Delaware, Newark, DE 19716, USA
[b] Regeneron Pharmaceuticals, Inc., Tarrytown, NY 10591, USA

ARTICLE INFO

Keywords:
Sea urchin
Blastocoelar cells
Pigment cells
Post-transcriptional regulation

ABSTRACT

MicroRNAs regulate gene expression post-transcriptionally by destabilizing and/or inhibiting translation of target mRNAs in animal cells. MicroRNA-124 (miR-124) has been examined mostly in the context of neurogenesis. This study discovers a novel role of miR-124 in regulating mesodermal cell differentiation in the sea urchin embryo. The expression of miR-124 is first detectable at 12hours post fertilization at the early blastula stage, during endomesodermal specification. Mesodermally-derived immune cells come from the same progenitor cells that give rise to blastocoelar cells (BCs) and pigment cells (PCs) that must make a binary fate decision. We determined that miR-124 directly represses *Nodal* and *Notch* to regulate BC and PC differentiation. miR-124 inhibition does not impact the dorsal-ventral axis formation, but result in a significant increase in number of cells expressing BC-specific transcription factors (TFs) and a concurrent reduction of differentiated PCs. In general, removing miR-124's suppression of *Nodal* phenocopies miR124 inhibition. Interestingly, removing miR-124's suppression of *Notch* leads to an increased number of both BCs and PCs, with a subset of hybrid cells that express both BC- and PC-specific TFs in the larvae. Removal of miR-124's suppression of *Notch* not only affects differentiation of both BCs and PCs, but also induces cell proliferation of these cells during the first wave of Notch signaling. This study demonstrates that post-transcriptional regulation by miR-124 impacts differentiation of BCs and PCs by regulating the Nodal and Notch signaling pathways.

1. Introduction

MicroRNAs (miRNAs) are short non-coding RNAs that post-transcriptionally regulate gene expression by binding to their target transcripts to induce degradation and/or inhibit translation in animal cells (Bartel, 2004, 2018; Bhaskaran and Mohan, 2014; McGeary et al., 2019). miRNAs are involved in a variety of different biological processes, including cell specification, cell differentiation, cell proliferation, apoptosis, and oncogenesis (Alberti and Cochella, 2017; Anglicheau et al., 2010; Bartel, 2009; Fan et al., 2013; Kobayashi et al., 2015; Yang and Qi, 2020). Most of the research conducted on miR-124 has been in the context of neurogenesis, neural homeostasis, and various cancers (Cai et al., 2018; Ghafouri-Fard et al., 2021; Hou et al., 2015; Konrad and Song, 2022). To date, relatively little is known about the regulatory role of miR-124 in early embryogenesis. A prior study demonstrated that in *Ciona* (sea squirt), miR-124 suppresses ectodermal *Macho1*, which encodes a major transcription factor (TF) that promotes muscle development, to ensure that only neuronal transcripts are expressed in the ectoderm (Chen et al., 2011). Similarly, miR-124 has also been found to inhibit *Dlx5* (encodes a TF that promotes osteoblast development), to prevent myogenic differentiation in the ectoderm (Qadir et al., 2014). These studies reveal a potential role of miR-124 in mesodermal cell specification and differentiation.

To understand the function of miR-124 in mesodermal cell specification and differentiation, we used the purple sea urchin embryo (*Strongylocentrotus purpuratus*) as a model. With its well-defined gene regulatory works, we searched for miR-124 binding site within select signaling pathway components and transcription factors that are known to be involved in the development of mesodermally-derived cells, including muscle, multipotent cells, BCs, and PCs (Table S1). We identified potential miR-124 binding sites within *Nodal*, which is critical for dorsal-ventral axis formation and specification of mesodermally-derived

* Corresponding author.
E-mail address: jsong@udel.edu (J.L. Song).
[1] Equal contribution.
[2] Current address: Departments of Neurology and Neuroscience, Columbia University, Taub Institute on Alzheimer's Disease and the Aging Brain, USA.

https://doi.org/10.1016/j.ydbio.2023.06.017
Received 16 January 2023; Received in revised form 27 May 2023; Accepted 22 June 2023
Available online 5 July 2023

immune cells, including the blastocoelar cells (BCs) and pigment cells (PCs) (Angerer et al., 2011; Bessodes et al., 2012; Duboc et al., 2010). Additionally, we have previously identified miR-124 to directly suppress *Notch*, which is critical for neural development, as well as development of all non-skeletogenic mesenchyme cells (NSM) of the sea urchin embryo, giving rise to multipotent cells, muscle cells, BCs, and PCs (Konrad and Song, 2022; Materna and Davidson, 2012; Ohguro et al., 2011; Peterson and McClay, 2005; Range et al., 2008). We have previously shown that miR-124 perturbation results in transient structural defects in muscle fibers around the gut and a delay in formation of coelomic pouches that house the multipotent stem cells (Konrad and Song, 2022). The development of BCs and PCs are regulated by Delta/Notch signaling and Nodal signaling pathways (Croce and McClay, 2010; Duboc et al., 2010; Materna and Davidson, 2012; Materna et al., 2013; Sherwood and McClay, 1999). Since we identified potential miR-124 binding sites within *Nodal* and previously observed that miR-124 directly inhibits *Notch*, we focus on examining the post-transcriptional regulation of miR-124 on Nodal and Notch signaling pathways in mediating the development of mesodermally-derived BC and PC immune cells.

Notch signaling occurs in two waves during early development (Ohguro et al., 2011; Peterson and McClay, 2005; Range et al., 2008; Sherwood and McClay, 1999) (Fig. 1A). Prior to the 16-cell stage, ubiquitously expressed *HesC* represses *Alx1, Tbr, Ets1,* and *Delta* (Ettensohn and McClay, 1988; Ettensohn and Ruffins, 1993; Minokawa, 2017). When nuclear β-catenin protein becomes posteriorly restricted and enters the nuclei of micromeres of 32-cell stage embryo, it transcriptionally activates *Pmar1* in the micromeres (Revilla-i-Domingo et al., 2007; Sampilo et al., 2018; Weitzel et al., 2004). Pmar1 inhibits *HesC* to de-repress the expression of *Alx1, Tbr, Ets1* and initiates the first wave of Delta/Notch signaling (Croce and McClay, 2010; Ettensohn and Ruffins, 1993; Peterson and McClay, 2005; Range et al., 2008; Revilla-i-Domingo et al., 2007; Ruffins and Ettensohn, 1996; Sharma and Ettensohn, 2011; Sherwood and McClay, 1999; Weitzel et al., 2004). The first wave of Delta/Notch signaling is important for activating endomesodermal specific TFs in the posterior end of the embryo and establishing the endomesodermal segregation (Croce and McClay, 2010; Materna and Davidson, 2012; Peter and Davidson, 2011; Peterson and McClay, 2005; Range et al., 2008; Sherwood and McClay, 1999).

The expression of *Delta* in the large micromeres, which give rise to the primary mesenchyme cells (PMCs), activates Notch in the neighboring presumptive mesodermally-derived BC and PC progenitor cells to transcriptionally activate *Gcm* (Croce and McClay, 2010; Peterson and McClay, 2005; Range et al., 2008; Sherwood and McClay, 1999). Hours later, *Nodal* expression becomes restricted in the ectoderm on the ventral (oral) side of the embryo to specify the dorsal-ventral axis where it activates ventral genes, such as *Gsc*, and dorsal genes, such as *Tbx2/3* (Cavalieri and Spinelli, 2014; Duboc et al., 2010; Floc'hlay et al., 2021). Shortly after ventral-dorsal specification, Nodal signaling activates TF *Not*, which expands its expression from the ventral ectoderm into the endomesoderm to subsequently activate BC-specific TFs, including *Ese* and *Scl*, and inactivates *Gcm* on the ventral side of the embryo (Materna et al., 2013; Ohguro et al., 2011). This results in *Gcm* expression restricted to the dorsal side of the NSM (Croce and McClay, 2010; Materna and Davidson, 2012; Materna et al., 2013; Range et al., 2008; Solek et al., 2013). Thus, the BCs in the ventral side become specified first by Nodal signaling (Bessodes et al., 2012; Croce and McClay, 2010; Duboc et al., 2010; Materna and Davidson, 2012; Materna et al., 2013; Ohguro et al., 2011).

Prior to the ingression of specified PMCs into the blastocoel of the early mesenchyme blastula, the PMCs express *Delta* and continue to signal through Notch expressed on the BCs and PCs. The second wave of Delta/Notch occurs during skeletogenic cell ingression into the blastocoel at 17-22hpf (Croce and McClay, 2010; Ohguro et al., 2011; Peter and Davidson, 2011; Peterson and McClay, 2005). The Delta/Notch signaling pathway further induces all NSMs to differentiate, including the PCs, which express *Pks1* (Croce and McClay, 2010; Range et al., 2008). BCs and PCs express *Delta* to signal through Notch expressed by the small micromeres to induce them to become the multipotent cells (Li et al., 2013; Materna et al., 2013; Range et al., 2008). The second wave of Notch signaling completes differentiation of all NSMs and is especially critical for the differentiation of small micromeres into multipotent stem cells and muscle cells (Materna and Davidson, 2012; Sweet et al., 2002).

The pigment cell marker, *Gcm*, is expressed throughout the ring of NSM cells (Ransick et al., 2002). Fully differentiated PCs are the first immune cell type to ingress into the blastocoel at the mesenchyme blastula stage (Buckley and Rast, 2017; Ho et al., 2017). At the gastrula stage, they migrate to the outer edges of the ectoderm to perform immune functions, such as phagocytosing invading bacteria (Buckley and Rast, 2017). A subset of pigment cells enters the blastocoel at sites of wounding or infection and are similar to red spherule cells which mediate wound healing and immune response in adults (Smith et al., 2010; Solek et al., 2013). Later on, the oral NSM, which gives rise to the BCs, is specified through the co-expression of *GataC*, *Scl*, and *Erg* (Solek et al., 2013). BCs ingress after PCs from the tip of the archenteron and differentiate into several blastocoelar cell types (Hibino et al., 2006; Ho et al., 2017; Ruffins and Ettensohn, 1996; Sherwood and McClay, 1999; Solek et al., 2013; Tamboline and Burke, 1992). Four types of BCs have been characterized by their shape, including globular, filopodial, ovoid, and amoeboid shape (Ho et al., 2017; Nair et al., 2005), of which, *185/*333 has been used to detect mature differentiated filopodial cells and *MacpfA2* has been used to detect globular cells (Ho et al., 2017).

In this study, we focus on the role of miR-124 in mesodermal specification and differentiation of the immune cells. We first determine the timing of BC and PC specification. We identify that miR-124 plays a novel and critical role in immune cell development through its regulation of Nodal and Notch signaling pathways. miR-124 inhibition results in increased number of mature BCs and a concurrent decrease in the number of differentiated PCs. We present evidence that miR-124's regulation of *Nodal* and *Notch* modulate BC and PC differentiation and cell proliferation. Our work contributes to the understanding of post-transcriptional regulation mediated by miR-124 in mesodermal development and suggest that miR-124 may have broader regulatory role in other tissue development in addition to neural development.

2. Results

2.1. miR-124 inhibition results in normal skeletal development

Since the mesoderm gives rise to the PMCs which are the only cells that produce larval skeleton (Ettensohn and Ruffins, 1993; McClay et al., 1983), we examined the effect of miR-124 perturbation on the PMCs. We did not observe a significant change in the length of the dorsoventral connecting rods (DVCs) produced by the PMCs or a significant difference in PMC patterning between the control and miR-124 inhibitor-injected embryos (Fig. S1). Thus, miR-124 does not regulate skeletal development.

2.2. Blastocoelar cells are specified before pigment cells

The NSM gives rise to multipotent stem cells, muscle cells, BCs, and PCs (Ettensohn and Ruffins, 1993; McClay et al., 1983). The early specification of NSM has been well studied throughout the sea urchin community using two species of sea urchin: *Strongylocentrotus purpuratus* and *Lytechinus variegatus*. Interestingly, these two species of sea urchin are extremely similar in development; however, their order and timing of the NSM specification is different. In *L. variegatus*, the PCs are specified before the BCs, and in *S. purpuratus* that we examine in this study, BCs are specified before the PCs (Duboc et al., 2010; Materna and Davidson, 2012; Materna et al., 2013; Ohguro et al., 2011; Rizzo et al., 2006; Sherwood and McClay, 1999). In the purple sea urchin (*S. purpuratus*), it has previously been observed using colormetric RNA *in situs* that PCs specify at ~10hpf using *GataE* as a marker, before BCs specify at ~15hpf

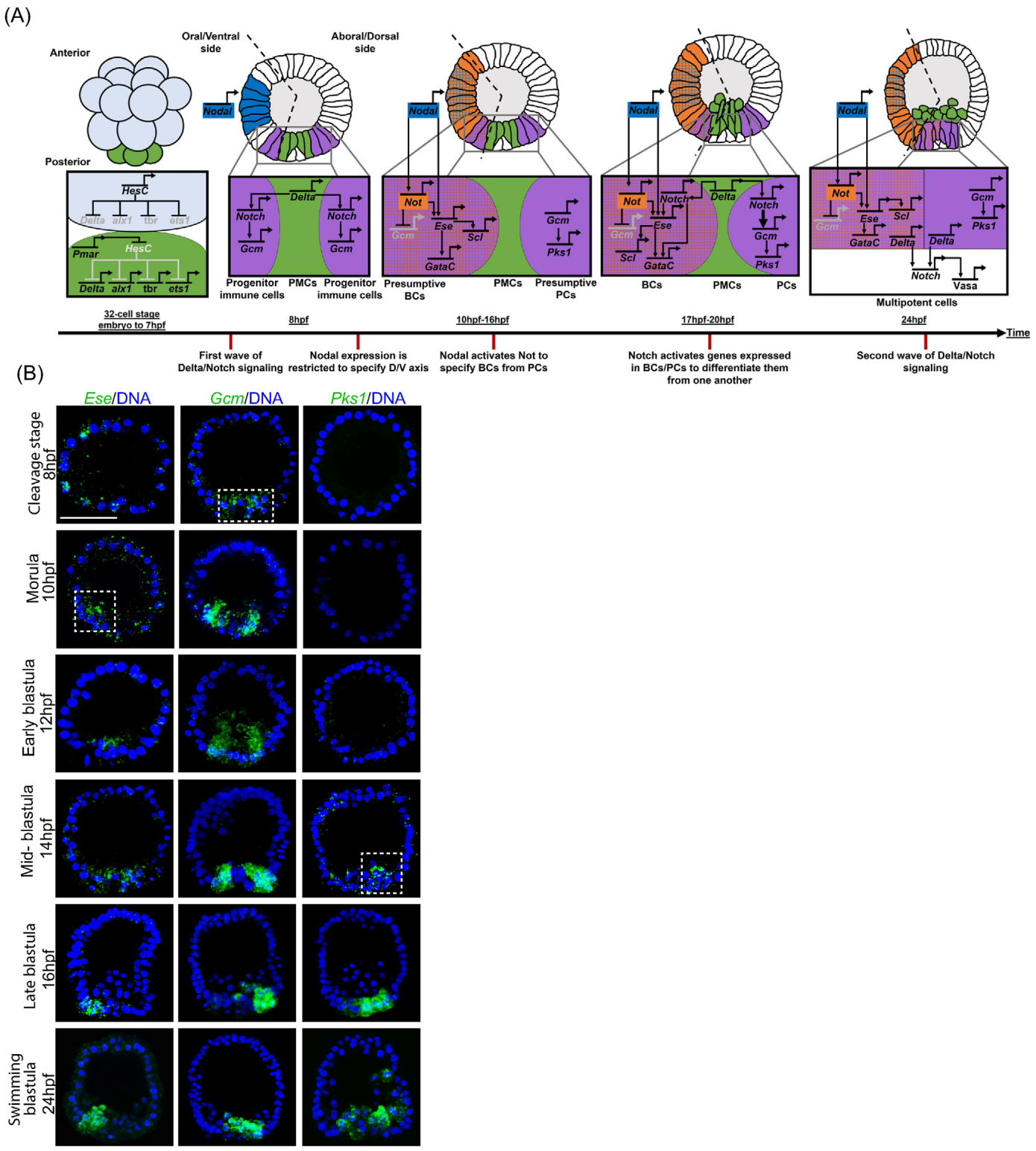

Fig. 1. Blastocoelar cells are specified before pigment cells. (A) Schematic of combined work from our research and others to demonstrate how blastocoelar and pigment cells specify and differentiate in the purple sea urchin. Mesodermal development is initiated by the activation of *Pmar* in the large micromeres that will become the primary mesenchyme cells (PMCs). Pmar inactivates *HesC* to allow the expression of *Delta* in the presumptive PMCs to initiate the first wave of Notch signaling that will initiate the specification of the presumptive NSM. Nodal signaling will first set up dorsal-ventral axis prior to 10hpf (hours post fertilization) (morula) and then activates Not to allow specification of BCs. Lastly, before ingression of PMCs into the blastocoel, Delta will signal to Notch in the BCs and PCs to further activate genes important for their differentiation prior to their ingression into the blastocoel to perform their immune functions (Duboc et al., 2010; Range et al., 2008; Revilla-i-Domingo et al., 2007). (B) FISH was performed at several time points to reveal the timing of BC and PC specification in the purple sea urchin. *Gcm* is expressed in BC and PC progenitor cells starting at 8hpf. *Ese* is used to follow specified BCs, and *Pks1* is used to follow specified PCs. *Gcm* becomes restricted in PCs to the aboral side at 14-16hpf (mid-to late blastula). Initiation of specification of BCs begins with *Ese* expression at 10hpf (morula) (indicated by the dotted box), and specification of PCs begins when *Pks1* is expressed at detectable levels at 14hpf (mid-blastula) (indicated by the dotted box). A range of 3–8 confocal images slices were compiled into a single maximum projection image. Scale bar = 50 μm. 3 biological replicates.

using *Ese* as a marker (Materna and Davidson, 2012; Materna et al., 2013). However, real time, quantitative PCR (qPCR) data from the same paper indicated that *Pks1* and *Z166* (PC-specific genes) are not expressed until ~15hpf (mid-blastula), while *Ese* (BC-specific TF) is expressed by ~10hpf (morula) (Materna et al., 2013). Thus, we determine the detailed timing of BC and PC specification, using *Gcm* to follow BC and PC progenitor cells, *Ese* to follow BCs, and *Pks1* to follow PCs, using Fluorescent *in situ* hybridization (FISH) (Fig. 1B). Our results indicate that the expression of BC-specific *Ese* was detected at 10hpf (morula), prior to the expression of PC-specific gene *Pks1*, which was detected at 14hpf (mid-blastula). At around 16hpf (late blastula), *Gcm* expression became restricted to the dorsal (aboral) side of the embryo, indicating PC specification (Fig. 1B). Thus, our results indicate that BCs are specified prior to PCs in *S. purpuratus* (Fig. 1). These data are consistent with another species of sea urchin, *Hemicentrotus pulcherrimus,* where BCs are specified before PCs (Ohguro et al., 2011).

2.3. *miR-124 is expressed during Nodal signaling and the first wave of Notch signaling*

To understand how miR-124 regulates Nodal and Notch signaling pathways during early development, we conducted a detailed temporal and spatial expression of miR-124 (Fig. 2). Using qPCR, we observed that miR-124 is expressed at 18hpf (hatched blastula) (Fig. 2A). Thus, miR-124 is not expressed during dorsal-ventral axis formation and early specification of BCs and PCs prior to 12hpf (early blastula). However, miR-124 is expressed at 18hpf (hatched blastula), when Notch signaling is important for activating a positive feedback loop in the BCs and PCs to further differentiate these cells (Range et al., 2008).

We also examined the spatial and temporal expression of miR-124 (Fig. 2B). In general, we observed a similar miR-124 expression profile as the qPCR data in that miR-124's expression peaks at the late and hatched blastula (Fig. 2A and B). We included additional developmental time points and revealed that miR-124 is expressed at detectable levels at 12hpf (early blastula) which is after dorsal-ventral axis formation, peaks at 16hpf (late blastula), and subsides after 18hpf (hatched blastula). While miR-124 is expressed in most cells, it seems to be more enriched in the dorsal/aboral side of the embryo, where *Not* (ventral ectoderm marker) is not expressed (Fig. 2C). This asymmetric expression likely persists to the swimming blastula stage at 24hpf (Fig. 2B and C). We also observed *Notch* to enrich in the posterior region of the late blastula (16hpf) embryo, where miR-124 seems to co-express with *Notch* in the posterior NSM cells (Fig. 2D).

Based on the qPCR and FISH data, results indicate that miR-124 is expressed between 12 and 18hpf during which a time when *Nodal* has transcriptionally activated *Not* (when BCs are being specified) and when Notch signaling has activated genes important for BC and PC differentiation (Figs. 1 and 2) (Burke, 2022; Ohguro et al., 2011).

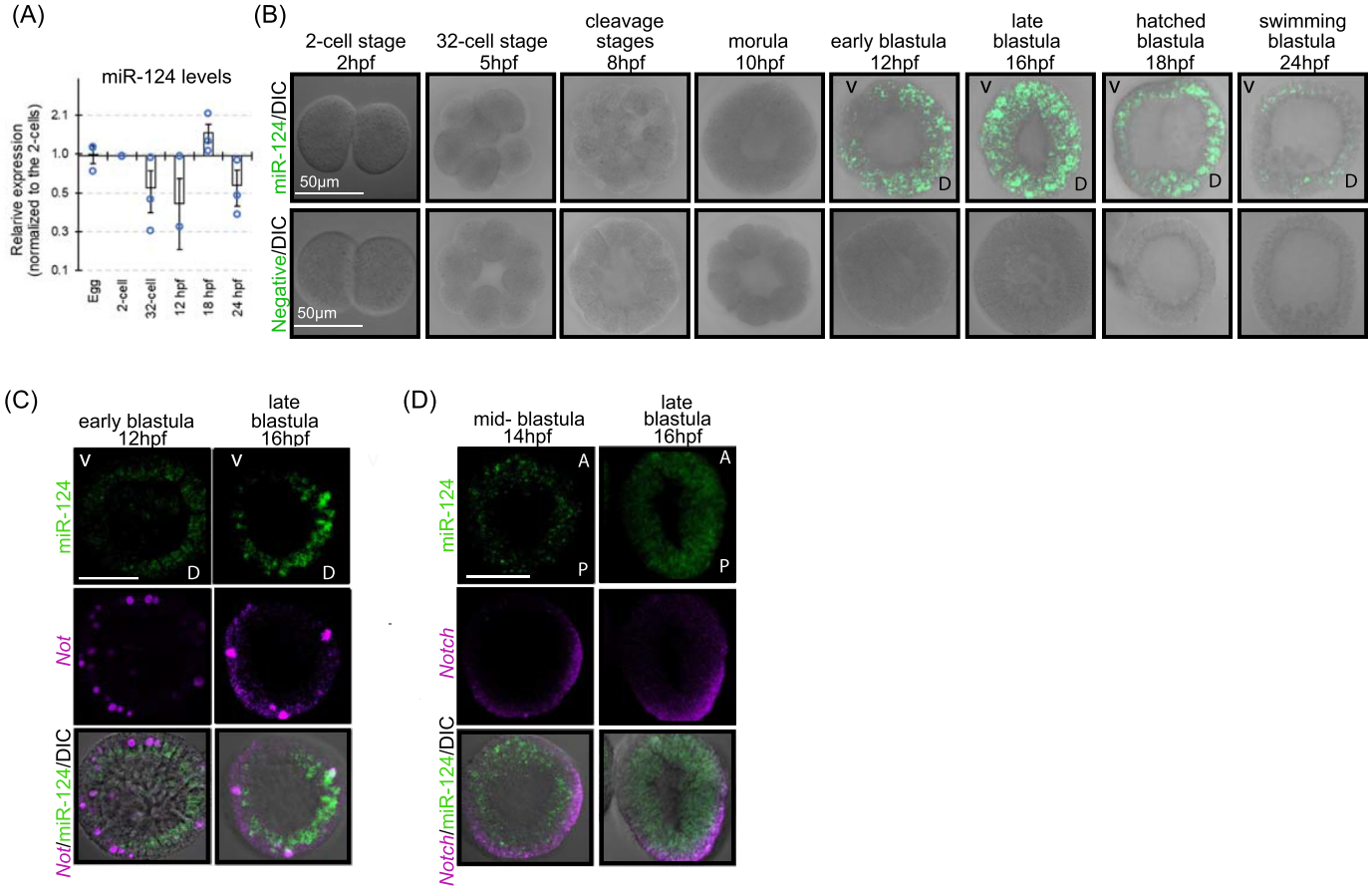

Fig. 2. miR-124 is expressed during Nodal signaling and towards the end of the first wave of Notch signaling. (A) miR-124 qPCR was performed at different developmental timepoints. Individual blue circles represent the three replicates, with the bar graph indicating the averages. SEM is graphed. miR-124 is expressed at 18hpf. (B) Embryos were collected at different developmental timepoints and hybridized with either miR-124 or the scrambled control LNA RNA probe. The expression of miR-124 is first detectable at 12hpf, peaks at 16hpf, and subsides after 18hpf. V = ventral ectoderm; D = dorsal ectoderm (C) Double FISH with miR-124 (green) and ventral marker *Not* (magenta) experiment indicates that miR-124 is more enriched on the dorsal/aboral side of the embryo. This asymmetric expression of miR-124 persists to the 24hpf (swimming blastula stage). *Not* seems to be highly expressed in cells that are dividing. (D) Double FISH with miR-124 (green) and *Notch* (magenta) was performed. miR-124 co-expresses with *Notch* in NSM cells in late blastula stage. A = anterior; P = posterior. For each developmental stage, we examined approximately 40 embryos. At least 3 biological replicates were performed. Single confocal images are presented.

2.4. miR-124 inhibition results in decreased number of pigment cells and increased number of blastocoelar cells

To examine the effect of miR-124 on mesodermally-derived immune cells, we injected control or miR-124 inhibitor into newly fertilized eggs. Of note is that embryos injected with the miR-124 inhibitor have a significant reduction of miR-124 levels, compared to injected control embryos, indicating the effectiveness of the inhibitor (Konrad and Song, 2022).

Upon miR-124 perturbation, we observed a two-fold decrease in the number of PCs compared to the control larvae (Fig. 3A). We were able to rescue the decrease of PCs in miR-124 inhibitor-injected embryos, by co-injecting miR-124 inhibitor with miR-124 mimic. Even though the rescue is not complete, we observed an approximately 75% rescue of the PCs control embryos compared to the miR-124 inhibitor-injected embryos (Fig. 3A). We also examined the number of PCs via Sp1 immunolabeling and observed similar changes in the number of PCs compared to the counting of the pigmented cells using bright field (Fig. 3B). These results indicate that miR-124 inhibition induces a loss of differentiated PCs and not just the pigmentation of the cells (Fig. 3A and B).

Since PCs and BCs are derived from the same progenitor cells, we also examined the number of BCs. To identify as many mature BC as possible, we used both the *185/333* and *MacpfA2* RNA *in situ* probes together to detect filopodial and globular BCs, respectively (Ho et al., 2017). We observed that miR-124 perturbation leads to a 1.5-fold increase in the number of mature BCs expressing *185/333* and *MacpfA2* (Fig. 3C). Interestingly, the morphology of the BCs is also altered to have more extensive filopodial structures. These results indicate that miR-124 regulates the differentiation of BCs and PCs, resulting in increased BCs at the expense of PCs.

2.5. miR-124 directly suppresses Nodal and affects Not expression

We bioinformatically identified a potential miR-124 binding site within the coding sequence (CDS) of *Nodal*. Previously it has been observed that even though miRNA binding sites are usually found in the 3′UTR, miRNAs can bind to all parts of the transcript (Chakraborty and Nath, 2022; Hausser et al., 2013). To test if miR-124 directly regulates *Nodal*, its CDS were cloned downstream of *Renilla* Luciferase (*RLuc*) construct. Site-directed mutagenesis was used to delete the entire predicted miR-124 seed sequence from the *Nodal* CDS. Firefly (FF) luciferase flanked by *β-globin* UTRs was used as an injection control. The dual luciferase assay results indicated a significant increase of luciferase activity in the *RLuc* fused with *Nodal* CDS with deleted miR-124 seed, in comparison to the *RLuc* fused with *Nodal* CDS with wild type miR-124 seed, demonstrating that miR-124 directly suppresses *Nodal* (Fig. 4A).

Upon miR-124 inhibition, we observe that the expression domain of *Not* expanded within the ectoderm as well as into the ventral

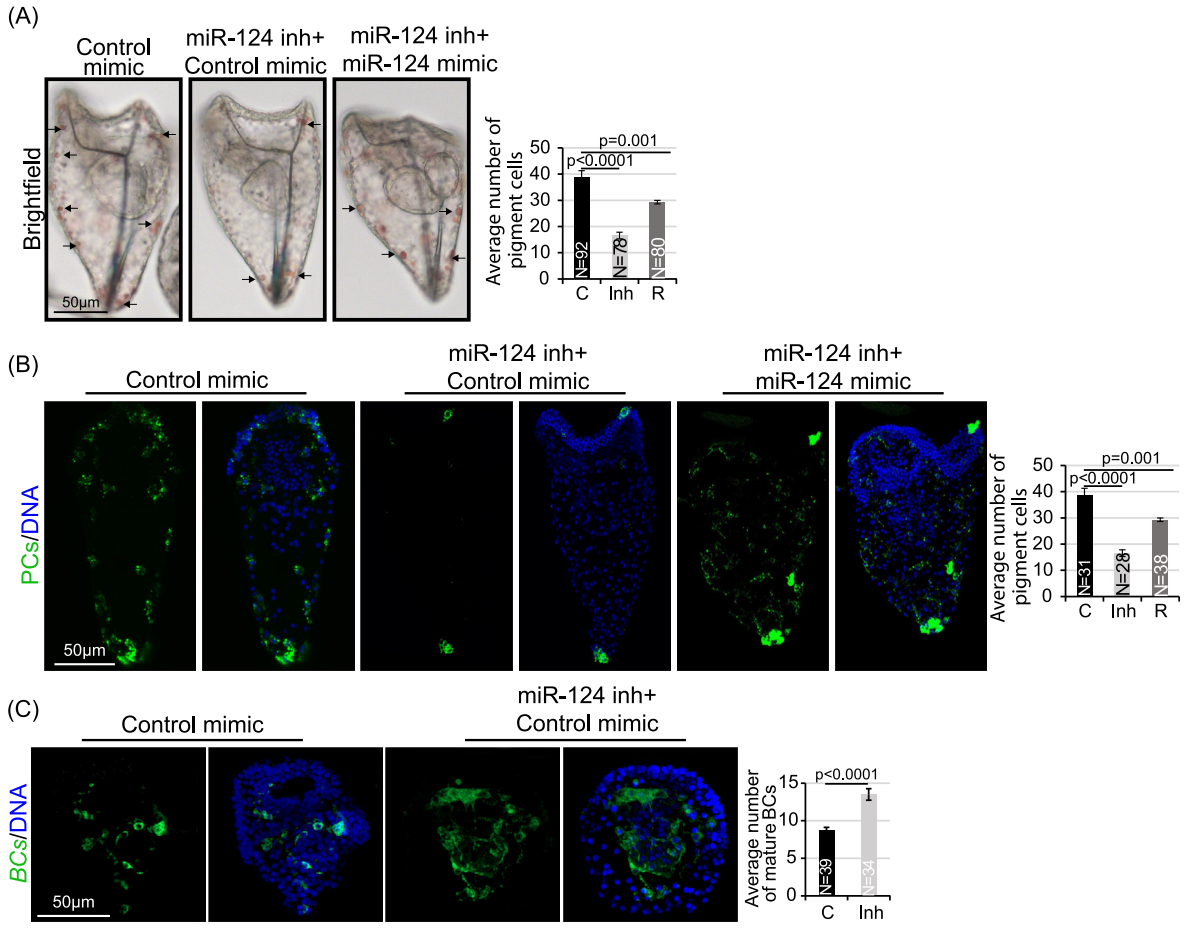

Fig. 3. Inhibition of miR-124 results in increased BCs at the expense of differentiated PCs. (A) The number of PCs were counted based on their natural purple pigmentation. miR-124 inhibitor-injected larvae had decreased differentiated PCs compared to the control embryos. 3 biological replicates. Black arrows point to some PCs. (B) PCs were immunolabeled with PC-specific Sp1 antibody (green) and counterstained with DAPI to label DNA (blue). We observed a similar decrease in PCs in the miR-124 inhibitor-injected larvae in comparison to the controls. C = control; Inh = miR-124 inhibitor; R = miR-124 inhibitor co-injected with miR-124 mimic. 3 biological replicates. Student T-test. Maximum intensity projection of Z-stack confocal images is presented. (C) miR-124 inhibitor-injected larvae had more *185/333* and *MacpfA2*-positive BCs (green) than the control. Larvae were counterstained with DAPI (blue). C = control; Inh = miR-124 inhibitor. 3 biological replicates. Student T-test. Maximum intensity projection of Z-stack confocal images is presented.

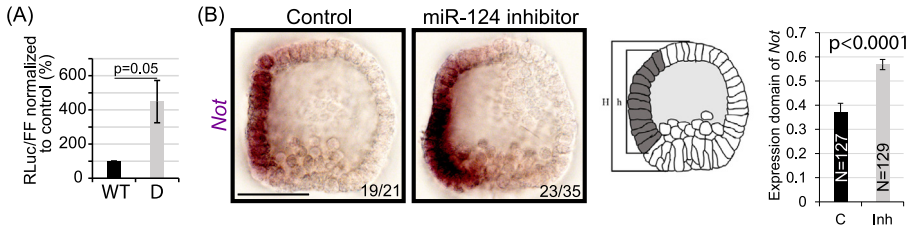

Fig. 4. *Nodal* is a direct target of miR-124 and miR-124 inhibition leads to expanded *Not* expression domain. (A) Dual luciferase assay results indicated that miR-124 directly suppresses *Nodal*. Each biological replicate contained 50 embryos. 3 biological replicates. SEM is graphed. Student's t-test was used. WT = wild type miR124 site; D = deleted miR-124 site. (B) miR-124 inhibitor-injected blastulae had increased and expanded *Not* expression compared to the control. The expression domain of *Not* is measured from anterior to posterior region and presented as a ratio to the height of the embryo. 3 biological replicates. Scale bar = 50 μm.

endomesoderm (Fig. 4B). In the control, we observed that 90% (19/21) look similar to what is depicted in the image, whereas for the miR-124 inhibitor-injected embryos, we observed 66% (23/35) of embryos have expression domain of *Not* expanding into the ventral endomesoderm, with the remaining 34% of the embryos look similar to the control (Fig. 4B). We measured the expression domain of *Not* by taking the ratio of its anterior to posterior expression domain and the height of the embryo (h/H). Using this approach, we observed that the expression domain of *Not* is significantly expanded upon miR-124 inhibition (Fig. 4B). These data suggest that miR-124 suppresses *Nodal* to impact the expression of *Not* which may have downstream effects on the development of BCs and PCs.

2.6. *miR-124 directly suppresses Nodal to regulate immune cell development*

Nodal activates *Not* to subsequently activate BC-specific TFs, which include *Ese* and *Scl,* and inactivates *Gcm* on the ventral side of the embryo (Materna et al., 2013; Ohguro et al., 2011). Thus, Nodal signaling promotes differentiation of BCs prior to PCs (Materna et al., 2013; Ohguro et al., 2011). To determine the impact of removing miR-124's suppression of *Nodal*, we injected a morpholino-based target protector (TP) (Remsburg et al., 2019; Staton and Giraldez, 2011) that is complementary to the validated miR-124 binding site and flanking sequences within *Nodal.* Of note is that the designed *Nodal* TP was blasted against the sea urchin genome and is only homologous to *Nodal. Nodal* expression is restricted to the ventral ectoderm at ~10hpf to activate genes important for setting up the dorsal-ventral axis (Cavalieri and Spinelli, 2014; Molina et al., 2013). Later at ~12hpf, Nodal activates *Not*, leading to differentiation of BCs and PCs (Duboc et al., 2010; Li et al., 2013; Ohguro et al., 2011; Yaguchi et al., 2007). Upon removal of miR-124's suppression of *Nodal*, we observe a dose-dependent increase in the expression domain of BC-specific TF *Ese* and *Scl,* compared to the control (Fig. 5A). Concurrently, we also observed a significant decrease in expression domains of PC-specific TFs (*Gcm* and *Pks1*) (Fig. 5B). The increased expression domain of BC-specific TFs in blastulae correlated with an increased number of mature BCs (*185/333* and *MacpfA2*-positive) in *Nodal* TP-injected larvae compared to the control (Fig. 5C). In the larval stage, we observed a subsequent decrease in the number of differentiated PCs in *Nodal* TP-injected larvae compared to the control (Fig. 5D and E). In general, *Nodal* TP-injected larvae phenocopy what we observed in the miR-124 inhibitor-injected embryos. Overall, these results demonstrate that miR-124 regulates BC and PC specification, in part by suppressing *Nodal* and altering expressions of BC and PC-specific TFs.

2.7. *miR-124 directly suppresses Notch to regulate immune cell development*

Since we determined previously that miR-124 directly suppresses *Notch,* and *Notch* signaling regulates development of NSM (Konrad and Song, 2022; Ohguro et al., 2011), we tested the effects of removing miR-124 suppression of *Notch* on the development of BCs and PCs. Results indicate that removal of miR-124's suppression of *Notch* (*Notch* TP) leads to a significant increase in the expression domain of BC-specific genes, *Ese* and *Scl,* in the blastula stage (Fig. 6A, S2A). Interestingly, *Notch* TP-injected larvae also exhibited a significant and dose-dependent increase in the expression domain of PC-specific *Pks1* and *Gcm* (Figs. S2B and 6A). Using double FISH, we observe that BC-specific TF *Ese* in the *Notch* TP-injected blastula is mostly expressed on the ventral (oral) side of the embryo with some expansion into the dorsal (aboral) side where only PC-specific TFs should be expressed (Fig. 6A). At the same time, PC-specific TF *Pks1* seems to be expanded into the endomesoderm domain of the *Notch* TP-injected blastulae (Fig. 6A).

The increase in expression of BC-specific TFs correlated with increased number of *185/333* and *MacpfA2*-positive mature BCs in the larvae (Figs. 6B, S2C). We also observed an increase in differentiated PCs in *Notch* TP-injected larvae, based on *Pks1*-expressing cells, counting the number of pigmented PCs, as well as by immunolabeling PCs with Sp1 (Figs. 6B, S2D-E). Interestingly, of these increased BCs and PCs, we only observe 6% of these cells co-express BC and PC specific-TFs (3 hybrid in 52 BCs and PCs in *Notch* TP-injected embryos), when these cells should have already been differentiated from one another (Fig. 6B). Thus, these results indicate that a minor percentage of BC/PC hybrid cells co-express BC and PC-specific TFs.

2.8. *Removal of miR-124's suppression of Notch leads to increased proliferating cells*

The number of hybrid cells expressing both BC and PC-specific TFs does not explain the total number of increased BCs or PCs (Figs. 6B, S2C-E). Since prior studies have shown that Notch signaling pathway promotes cell proliferation in other systems (Baonza and Freeman, 2005; Demitrack et al., 2017; Kopan, 2012; Nusser-Stein et al., 2012), we tested if removal of miR-124's suppression of *Notch* induces cell proliferation of BCs and PCs. Notch signaling is known to induce further differentiation of BCs from PCs at 17hpf prior to ingression of PMCs into the blastocoel (Materna and Davidson, 2012; Ohguro et al., 2011; Range et al., 2008; Sweet et al., 2002), so we reasoned that if Notch signaling was going to activate cell proliferation in BCs and PCs, this may occur at around 17hpf. To test this hypothesis, we pulsed the embryos with ethynyl deoxyuridine (EdU) for 30 min to assay for cell proliferation at 16hpf. We then cultured the embryos to the swimming blastula stage (24hpf), when BCs and PCs should be specified (Croce and McClay, 2010; Range et al., 2008). In general, there was ~115% increase of proliferating cells in the *Notch* TP-injected blastulae (45 cells) compared to the control (39 cells) and a higher percentage of proliferating BCs and PCs in *Notch* TP-injected blastulae compared to the control (Fig. 7). We observed 31% (3.35/10.87) of BCs proliferate in *Notch* TP-injected blastulae versus 28% (2/7) of BCs proliferate in control TP-injected blastulae; 27% (6.6/24.8) of PCs proliferate in *Notch* TP-injected blastulae versus 24% (5/21) of PCs proliferate in control TP-injected blastulae (Fig. 7). These results suggest that removing miR-124's suppression of *Notch* correlated with increased cell proliferation during the tail end of the first wave of Notch signaling that may partly contribute to the increased BCs and PCs observed in the larval stage.

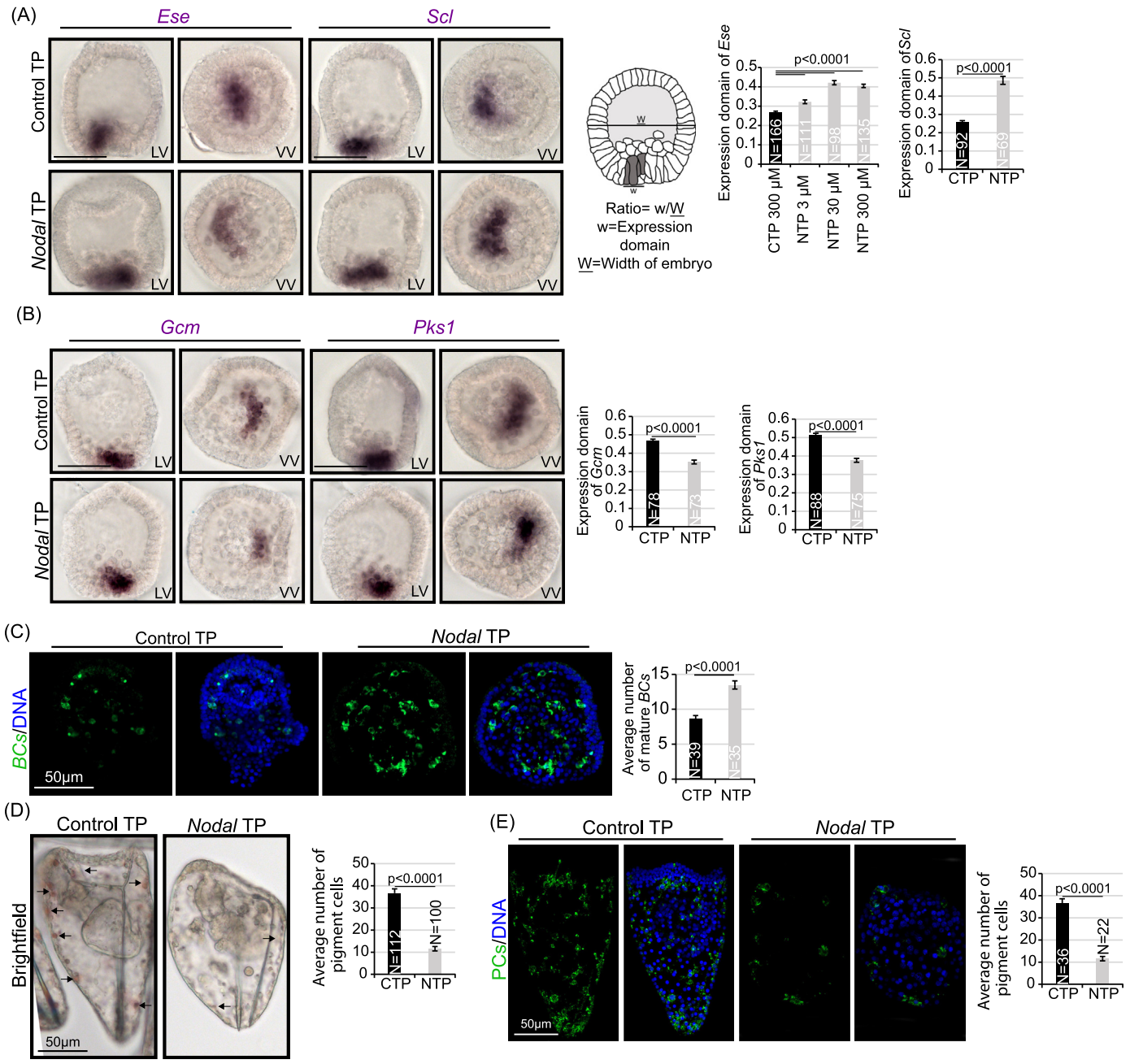

Fig. 5. Removing miR-124's direct suppression of *Nodal* results in increased BCs and a concurrent decrease in differentiated PCs. (A) *Nodal* TP-injected blastulae at 24hpf were subjected to RNA *in situ* hybridization with BC and PC-specific probes. A significant increase in BC-specific *Ese* and *Scl* expression domains was observed in the *Nodal* TP-injected embryos compared to the control TP-injected embryos. Schematic indicates the measurement of the expression domains. CTP=Control TP; NTP=*Nodal* TP. Student T-test. 3 biological replicates. (B) Control and *Nodal* TP-injected larvae were hybridized with BC markers *185/333* and *MacpfA2*. BCs are increased in *Nodal* TP-injected larvae. (C) *Nodal* TP-injected embryos have increased expression domains of PC-specific *Gcm* and *Pks1* at the blastula stage. (D) *Nodal* TP-injected embryos were cultured to 72hpf and exhibited 2-fold decrease in PCs. (E) PCs were immunolabeled with PC-specific Sp1 antibody (green) and counterstained with DAPI (blue). We observed a similar decrease in PCs in the *Nodal* TP-injected embryos in comparison to the controls. 3 biological replicates. Maximum intensity projection of Z-stack confocal images is presented. CTP=Control TP; NTP=*Nodal* TP. Student T-test is used for statistical analyses.

3. Discussion

In summary, we have identified a novel function of miR-124 in regulating specification and differentiation of mesodermally-derived immune cells in the sea urchin embryo, by suppressing Nodal and Notch signaling pathways. miR-124 is expressed between 12 and 18hpf to regulate *Nodal* after transcriptional activation of *Not* (when BCs are being specified) and also regulates *Notch* at 16-18hpf when Notch signaling activates genes important for BC and PC differentiation (Figs. 1A and 2). In general, miR-124 inhibition and blocking miR-124's suppression of *Nodal* resulted in similar phenotypes in that BCs were increased with concomitant decrease of PCs. Interestingly, blocking miR-124's suppression of *Notch* resulted in increased BCs and PCs, which may be in part as a result of Notch activating cell proliferation during the first wave of Notch signaling. Overall, our results reveal a novel role of miR-124 in regulating the development of mesodermally-derived BCs and PCs.

With miR-124 inhibition and removal of miR-124's suppression of *Nodal,* we did not observe apparent changes in dorsal-ventral axis formation mediated by Nodal (Fig. 4). The reason may be that miR-124 is

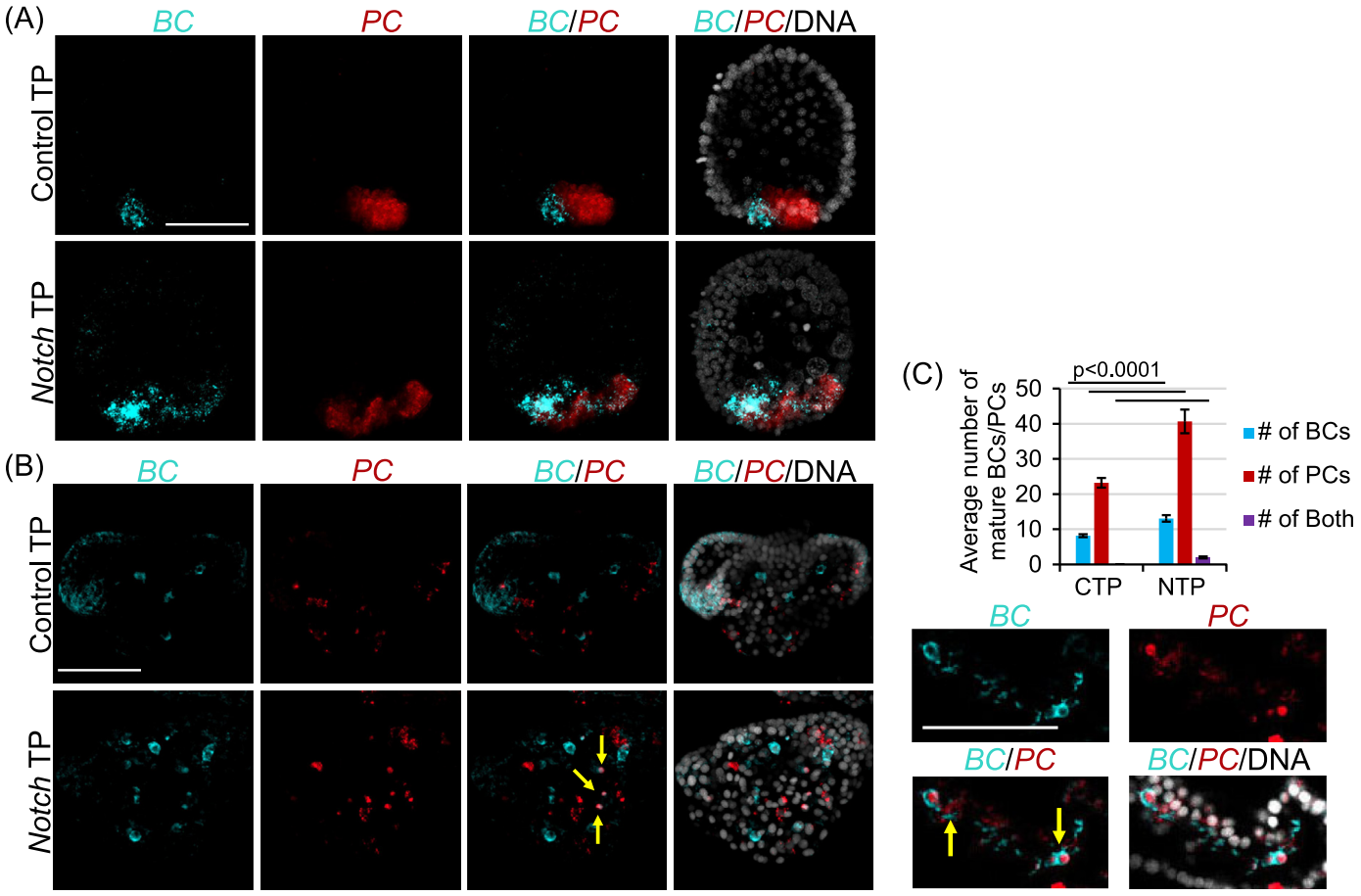

Fig. 6. Removal of miR-124's suppression of *Notch* results in expanded expression domains of BC and PC-specific TFs as well as the number of BCs and PCs. (A) Double FISH was conducted on *Notch* TP and Control TP-injected embryos at the blastula stage, using BC-specific TF *Ese* and PC-specific TF *Pks1* RNA probes. *Notch* TP-injected embryos exhibited an expanded expression domain of both *Ese* and *Pks1* during the blastula stage compared to the Control TP-injected embryos. (B) *Notch* TP-injected larvae have increased numbers of both *Ese*-positive cells and *Pks1*-positive cells, with a few hybrid cells expressing both markers (arrows). (C) Number of BCs, PCs, and hybrid cells (arrows) in Control and *Notch* TP-injected embryos are presented in a graph. Images indicate enlarged views of hybrid cells in *Notch* TP-injected embryos. CTP=Control TP (N = 38); NTP=*Notch* TP (N = 36). Student T-test. 3 biological replicates.

not expressed at sufficient levels until 12hpf (Fig. 2), when establishment of dorsal-ventral axis has occurred (Fig. 1A) (Molina et al., 2013). If miR-124 regulates dorsal-ventral axis formation through *Nodal* prior to 12hpf, we would expect morphologically symmetrical embryos with an embryonic mouth where it does not fuse with the ectoderm (Duboc et al., 2010; Duboc and Lepage, 2008; Ohguro et al., 2011; Suzuki and Yaguchi, 2018). Since embryos injected with miR-124 inhibitor and *Nodal* TP did not exhibit these typical dorsal-ventral morphological defects, these data indicate that miR-124 is not likely to regulate *Nodal* prior to 12hpf to impact dorsal-ventral axis formation (Figs. 3A and 5D).

Using *Nodal* and *Notch* TPs, we are able to dissect the regulatory function of miR-124 in modulating Nodal and Notch signaling pathways in BC and PC differentiation. Results from miR-124 inhibition and *Nodal* TP injection resulted in embryos with similar phenotypes, in that the number of BCs are significantly increased, with a concomitant decrease of the number of PCs (Figs. 3, 5D-E). A potential reason for why miR-124 inhibition preferentially promotes BC specification may be that miR-124 is first expressed at 12hpf (early blastula), during a time when Nodal activates *Not* to promote the specification of BCs (Figs. 1A, 2 and 4B). Blocking miR-124's suppression of *Nodal* with *Nodal* TP leads to increased BCs, suggesting that the level of Nodal signaling is responsive to miR-124's regulation and important for promoting BC specification, as the presumptive BCs in the embryo are exposed to Nodal signaling on the ventral side of the embryo. Thus, in miR-124 inhibitor and *Nodal* TP-injected embryos, the spatial position of presumptive BCs at the ventral side leads to more specified BCs at the expense of PCs.

Surprisingly, we observed that removal of miR-124's suppression of *Notch* results in an increase of both BCs and PCs (Fig. 6B, S2C-E). We propose that this is due to the fact that normally Notch signaling promotes all NSM fates, including both BCs and PCs (Fig. 1A). Therefore, when we remove miR-124's suppression of *Notch,* both cell types presumably receive increased Notch signaling. Results indicate that the number of cells of BCs and PCs are both increased, while the majority of these cells express cell-type specific TFs, with ~6% of the cells co-express both BC and PC specific TFs (Fig. 6B). One potential explanation could be that at this point, the BCs and PCs have not completely determined their fates, and that they are still expressing some shared transcripts that are transcriptionally responsive to Notch signaling. Interestingly, single cell RNA sequencing results indicate that lineage separations of some cells are gradual, indicating a more complex regulation that is needed to resolve a cell type (Massri et al., 2021). For example, primordial germ cells and PMCs become distinct cells early in cleavage stage of development (Croce and McClay, 2010; Oliveri et al., 2006; Peter and Davidson, 2011; Weitzel et al., 2004; Massri et al., 2021), whereas ectoderm-endoderm and endomesoderm cell states are observed in some cells prior to their lineage separation (Massri et al., 2021; Perillo et al., 2021). The

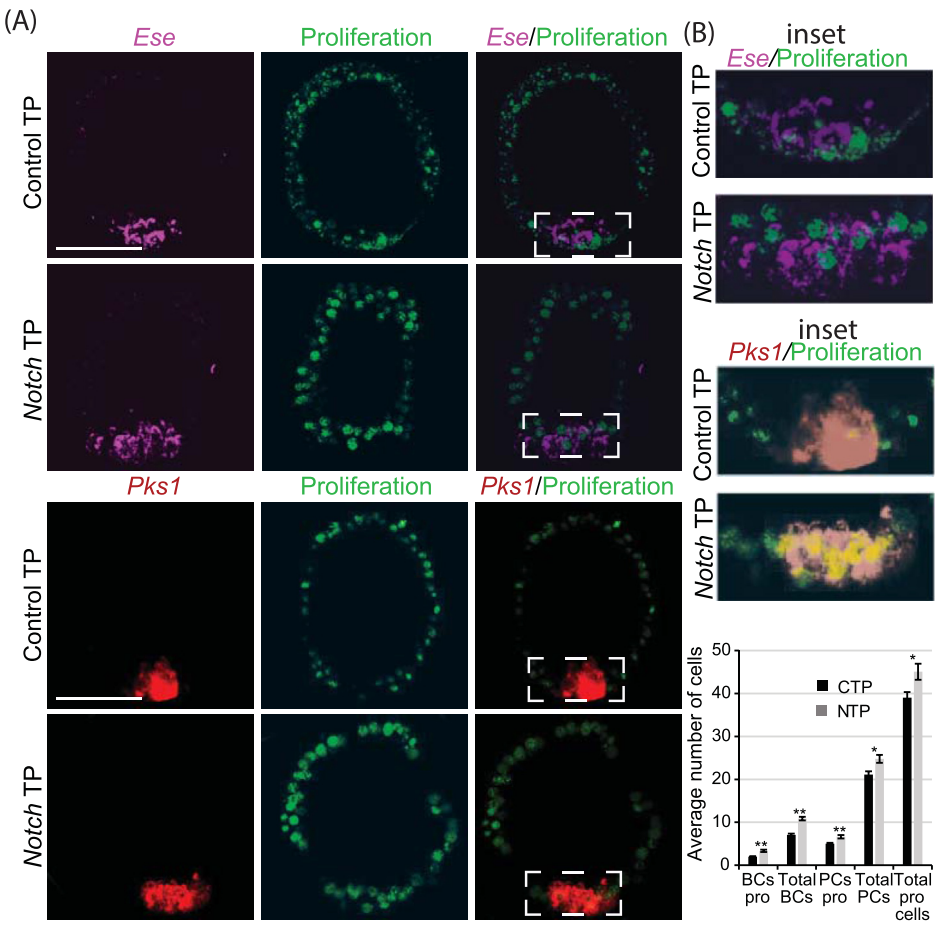

Fig. 7. Removal of miR-124's suppression of *Notch* results in an increased number of both BCs and PCs. (A) Embryos were incubated with Click-It EdU to detect cell proliferation for 30 min at 16hpf. At 24hpf, blastulae were fixed and incubated with BC and PC-specific markers and counterstained with DAPI to visualize DNA. *Notch* TP-injected embryos have more BCs and PCs that are undergoing cell division compared to control. Dotted white lines indicate the inset. (B) Inset images show enlarged areas of posterior region of the embryos. Graph indicates the number of proliferating BCs and PCs in Control and *Notch* TP-injected embryos. CTP = control TP (N = 39) and NTP=Notch TP (N = 31). Student T-test. 3 biological replicates. Maximum intensity projection of Z-stack confocal images is presented. *p < 0.05; **p < 0.001.

establishment of blastocoelar and pigment cell fates may be another example, where BCs and PCs share transcripts for an extended period of time prior to their final differentiation.

Another explanation is that the increased BCs and PCs may in part be due to increased cell proliferation. Notch signaling has been previously observed to promote cell proliferation (Baonza and Freeman, 2005; Hunter et al., 2016; Joshi et al., 2009). To test this idea, we examined the numbers of BCs and PCs after assaying for cell proliferation with EdU at 16hpf in *Notch* TP-injected embryos compared to the control TP-injected embryos (Fig. 7). At the blastula stage, we observed almost one additional doubling of BCs and PCs during 16–17hpf (~1.3 cell for BCs and ~1.6 cells for PCs) in *Notch* TP compared to control TP-injected embryos (Fig. 7). This result partially explains the increased numbers of these cells at the larval stage (Figs. 6B, S2C-E). These results are consistent with previous work that have found Notch signaling to induce *myc* and *p21* to promote cell proliferation in mice and human cell lines (Baonza and Freeman, 2005; Demitrack et al., 2017; Janardhanan et al., 2009; Kopan, 2012; Zhou et al., 2014). However, this increase of PCs during the blastula stage may not fully explain the doubling of PC numbers when we remove miR-124 suppression of *Notch* (Figs. 7, S2D-E). It has been proposed previously that in another species of sea urchin (*L. variegatus*), a third wave of Notch signaling may occur (Range et al., 2008), when Notch protein is expressed in the elongating gut during the gastrula stage as BCs and PCs ingress into the blastocoel; however, direct evidence of this has not been shown (Range et al., 2008). In addition, a small population of mitotic PCs in the larvae have previously been identified (*S. purpuratus*), although the mechanism of this is unknown (Perillo et al., 2021). Potentially, Notch signaling may promote cell proliferation in PCs in gastrula and larval stages. When we remove miR-124's suppression of *Notch*, it may activate some PCs to divide one more time during the larval stage, although we do not have direct evidence of this.

In addition, it is not clear if these fully differentiated BCs and PCs are functional upon an immune challenge. When these cells become activated, their morphology becomes round (Buckley and Rast, 2017; Ho et al., 2017). We did, however, observe that when we inhibit miR-124 and/or remove miR-124's suppression of *Notch*, BCs have longer filopodial extensions compared to the control (Figs. 2, 3C, S2C). Interestingly, when we just remove miR-124's suppression of *Nodal*, we do not observe this morphological change in the BCs (Fig. 5C). These results indicate that miR-124, upon its regulation of *Notch*, may impact morphological changes of BCs. It has been observed recently that Notch inhibitor-treated breast cancer cells have defects in filamentous actin, resulting in slower migration compared to the control (Liu et al., 2019). Thus, Notch signaling may promote actin structure to regulate cell migration. Since morphological changes of BCs may reflect their response and function during an immune response, it would be interesting to examine these embryos upon an immune challenge. However, the mechanism of how miR-124's regulation of *Notch* affects the morphology and cell migration of BCs needs to be further examined.

In summary, we observed that miR-124 inhibition and *Nodal* TP treatment lead to increased BCs with concomitant decrease of PCs, whereas *Notch* TP treatment lead to increased BCs and PCs (Fig. 8A). Based on our results and published literature, we propose a working model to explain miR-124's impact on BC and PC differentiation and proliferation (Fig. 8B). Early in development, BCs and PCs share the same progenitor cells. Both presumptive BCs and PCs express *Gcm* early in development, activated by the first wave of Notch signaling at the 32-cell stage. Initiation of BC and PC specification begins with Nodal signaling activating *Not* TF to subsequently activate BC-specific TFs and inhibit PC-specific TFs on the ventral side of the embryo. miR-124 is expressed in

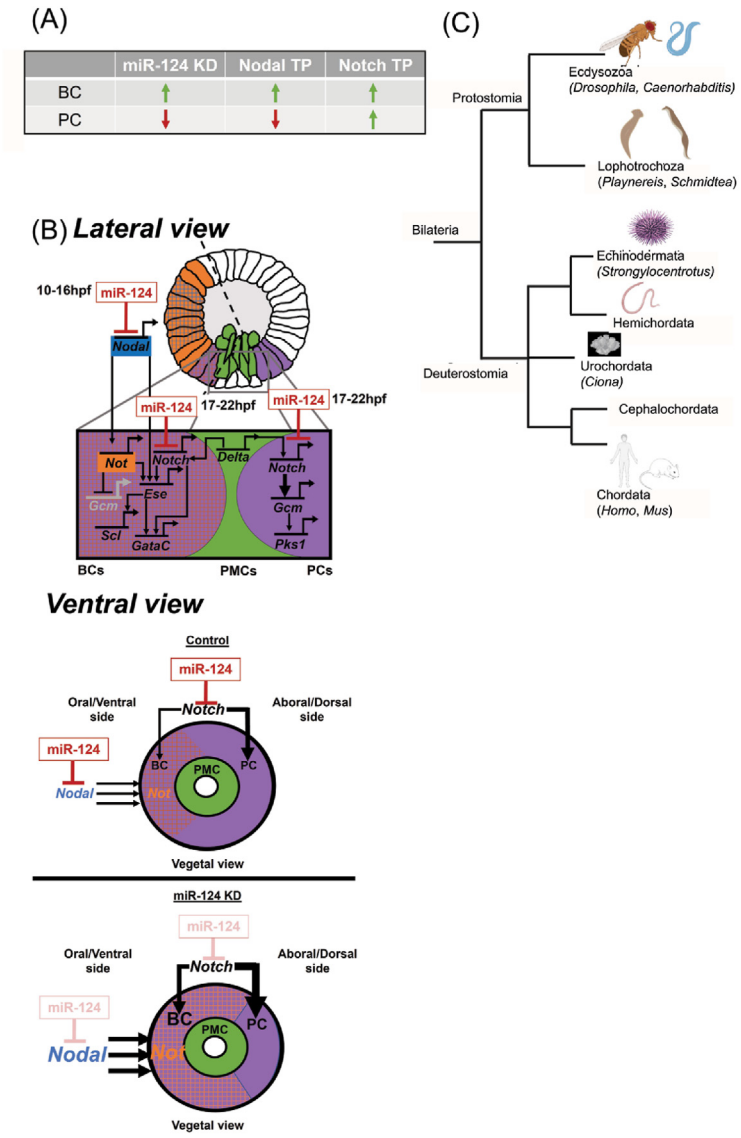

Species	miR-124 expression	References
Drosophila melanogaster	Brain, ventral nerve cord	Aboobaket al., 2005; Menzel et al., 2019
Caenorhabditis elegans	Ciliated nervous system	Clark et al., 2010
Strongylocentrotus purpuratus	Ubiquitous in early embryos; ciliary band in larva	Kalin and Song, 2022
Ciona intestinalis	Nervous system	Chen et al., 2011
Mus musculus	Brain (cerebellum, midbrain, cortex, rest of the brain)	Lagos-Quintana et al., 2002
Homo sapiens	Central nervous system; hematopoietic cells (low)	Sempere et al., 2004; Qin et al., 2016

Fig. 8. Model of regulatory mechanism of miR-124 in BC and PC development. (A) Summary of results. (B) Early in sea urchin development, BCs and PCs share the same progenitor cells. Initiation of specification of BCs begins with *Nodal* expression (blue) in the oral ectoderm that activates *Not* (orange), which activates BC-specific TFs and inhibits PC-specific TFs on the ventral/oral side of the embryo. miR-124 directly suppresses *Nodal* and *Notch*. miR-124 inhibition results in increased *Not*, leading to increased BCs at 14-16hpf. miR-124 continues its expression to 18hpf, when it regulates Notch signaling to impact BC and PC differentiation and proliferation. (C) Expression of miR-124 in various organisms throughout phylogeny is summarized. miR-124 is enriched in the neural system of all organisms.

most cells and is enriched at the dorsal ectoderm, where miR-124 directly suppresses *Nodal* soon after *Not* is activated to specify BCs. As a result of the proximity of BCs to the ventral/oral ectoderm, where they receive Nodal signaling and Not, the BCs are specified prior to the PCs (Figs. 1 and 8B). Removal of miR-124's suppression of *Nodal* promotes specification of BCs, potentially as a result of increased Nodal signaling between 12 and 18hpf (early blastula to hatch blastula stages), during a time when miR-124's expression is first detected (Fig. 8B). Consistent with this, we observed miR-124's expression is less on the ventral/oral side of the embryo to allow *Nodal* expression (Fig. 2B). Once these immune progenitor cells are exposed to increased Nodal signaling, then more BCs are formed at the expense of PCs, since they come from the same progenitor cells. Notch signaling at ~17-22hpf continues to promote the specification of both BCs and PCs. The expression of miR-124 peaks at 16hpf where it is less expressed in the ventral/oral side of the embryo and subsides during the time when Notch signaling activates genes that promote differentiation of BCs and PCs (Fig. 2B and C). In the late blastula stage (after 16 hpf), *Notch* becomes more restricted to the posterior end of the embryo where it co-expresses with miR-124 to regulate NSM differentiation (Fig. 2D). Upon removal of miR-124's suppression of *Notch*, the potential increase of Notch signaling promotes both BC and PC differentiation and cell proliferation. Overall, this work reveals a novel role of miR-124 in regulating mesodermal derived immune cell development.

4. Materials and methods

4.1. Animals

Adult *Strongylocentrotus purpuratus* were collected from the California coast (Pt. Loma Marine Invertebrate Lab or Marinus Scientific, LLC.). All animals and cultures were incubated at 15 °C in neutral sea water (NSW).

4.2. Microinjections

Injection solutions contained 20% sterile glycerol, 2 mg/mL 10,000

MW FITC lysine charged dextran (ThermoFisher Scientific, Waltham, MA), and various concentrations. For majority of the experiments, Control TP 30 μM, *Nodal* TP 30 μM and *Notch* TP 30 μM were used. Control, *Nodal* TP, and *Notch* TP were also injected at 3 μM and 300 μM to perform dose-response experiments. Hsa-miR-124-3p Locked Nucleic Acid (LNA) power inhibitor and Hsa-miR-124-3p miRCURY LNA miRNA mimic (Qiagen, Germantown, MD) were resuspended with RNase-free water to 100 μM. Based on previous dose-response results, we used 15 μM of the Hsa-miR-124-3p LNA power inhibitor for subsequent experiments. The Hsa-miR-124-3p miRCURY LNA miRNA mimic (Qiagen, Germantown, MD) was used at 15 μM with miR-124 inhibitor as well as the miRCURY LNA control miRNA mimic (Qiagen, Germantown, MD). For miR-124 inhibition experiments, we used FITC dextran (ThermoFisher Scientific, Waltham, MA) as an injection control. Microinjections were performed as previously described (Konrad and Song, 2022; Stepicheva and Song, 2014).

4.3. Fluorescence RNA in situ hybridization (FISH) and whole mount RNA in situ hybridization (WMISH)

The steps performed for FISH are described previously with modifications (Konrad and Song, 2022; Sethi et al., 2014). To generate WMISH RNA probes, we used PCR to amplify *Not, Gcm*, *Pks1*, *Ese*, *Scl,* and *MacpfA2* from sea urchin egg and embryonic cDNA of 24hpf, 48hpf, 72hpf. PCR primers were designed off sequences of these genes taken from Echionobase (Arshinoff et al., 2022). To generate the *Notch* RNA probe, we amplified a 1 Kb 3′UTR region off the *Notch* luciferase construct. The primers and enzymes used to linearize and make antisense probes are listed in Table S2. Primers were designed using the Primer3 program (Table S2). The 185-133 sequence was obtained from the Echionbase (Arshinoff et al., 2022) (+1 to +1031 of the CDS) was synthesized (Twist Biosciences, South San Francisco, CA). The steps performed for WMISH are as previously described (Konrad and Song, 2022; Song et al., 2012; Stepicheva et al., 2015). After WMISH, embryos were imaged using the Observer Z.1 microscope using the Axiocam 305 color camera (Number of Pixels: 2464 × 2056, Pixel size 3.45 × 3.45 μm) (Carl Zeiss Incorporation, White Plains, NY).

All FISH-labeled embryos were mounted using DAPI in MOPs-based buffer (Konrad and Song, 2022; Perillo et al., 2021; Song et al., 2012; Stepicheva et al., 2015) (NucBlue; Thermo Fisher Scientific, Waltham, MA). For quantification, embryos were imaged on Observer Z.1 microscope (Carl Zeiss Incorporation, White Plains, NY) with a 20× air lens with a numerical aperture 0.8 using the Axiocam MRm 1.4 MP camera (Number of Pixels: 1388 × 1040, Pixel Size: 6.45 μm × 6.45 μm) (Carl Zeiss Incorporation, White Plains, NY). For representative images, the embryos were imaged on Zeiss LSM 880 scanning confocal microscope or Zeiss LSM 980 multiphoton confocal microscope (Carl Zeiss Incorporation, White Plains, NY). The maximum intensity projections of Z-stack images were acquired with Zen software for representative images (Carl Zeiss Incorporation, White Plains, NY) and processed with Adobe Photoshop and Adobe Illustrator (Adobe, San Jose, CA).

4.4. Immunolabeling procedures

To assess miR-124 inhibitor induced phenotypes, we used antibodies against various cell types. We used 1D5 at 1:50 (McClay et al., 1983) to detect PMCs, and Sp1 at 1:200 (DSHB, Lot #3/9/12–32 μg/mL) (Gibson and Burke, 1985) to detect pigment cells. Embryos were fixed in 4% paraformaldehyde (PFA) (20% stock; EMS, Hatfield, PA) in artificial sea water overnight at 4 °C. Three 15-min 1× Phosphate Buffered Saline-Tween-20 0.05% (PBST) (Bio-Rad, Hercules, CA) washes were performed. Embryos were blocked with 4% sheep serum (MilliporeSigma, St. Louis, MO) for 1 h at room temperature. All embryos were incubated overnight with the primary antibodies at 4 °C in a blocking solution (4% sheep serum in PBST). Embryos were washed three times 15 min with PBST followed by incubation with secondary antibodies goat anti-mouse Alexa 488 or Alexa 647 at 1:300 for 1 h at room temperature (Thermo Fisher Scientific, Waltham, MA).

All immunolabeled embryos were mounted using DAPI in PBST buffer (NucBlue; Thermo Fisher Scientific, Waltham, MA). The 1D5 immunolabeled embryos were imaged on Observer Z.1 microscope (Carl Zeiss Incorporation, White Plains, NY) with a 40× air lens with a numerical aperture 1.2 using the Axiocam MRm 1.4 MP camera (Number of Pixels: 1388 × 1040, Pixel Size: 6.45 μm × 6.45 μm) (Carl Zeiss Incorporation, White Plains, NY). For Sp1 quantification, embryos were imaged on Observer Z.1 microscope (Carl Zeiss Incorporation, White Plains, NY) with a 20× air lens with a numerical aperture 0.8 using the Axiocam MRm 1.4 MP camera (Number of Pixels: 1388 × 1040, Pixel Size: 6.45 μm × 6.45 μm) (Carl Zeiss Incorporation, White Plains, NY). For representative images, the embryos were imaged on Zeiss LSM 880 scanning confocal microscope or Zeiss LSM 980 multiphoton confocal microscope (Carl Zeiss Incorporation, White Plains, NY). The maximum intensity projections of Z-stack of images were acquired with Zen software for representative images (Zeiss, White Plains, NY) and exported into Adobe Photoshop (Adobe, San Jose, CA) for further processing.

4.5. Cloning for luciferase reporter constructs

The CDS of *Nodal* were cloned using sea urchin cDNA with primers against the 3′UTR and or CDS (Table S2). Positive clones were sequenced (Genewiz Services, South Plainfield, NJ) and subcloned into *RLuc* as described previously (Stepicheva et al., 2015). The miR-124 seed sequence (5′-GTGCCTT-3′) was deleted from *Nodal's* CDS. Mutations were generated using the QuikChange Lightning Kit (Agilent Technologies, San Jose, CA). Clones were sequenced to confirm the presence of miR-124 binding site mutations or deletions (Genewiz Services, South Plainfield, NJ).

The CDS of *Nodal RLuc* reporter constructs primers and restriction enzymes and RNA polymerases used are listed in Table S2. *FF* was linearized using *Spe*I and *in vitro* transcribed with SP6 RNA polymerase (Stepicheva et al., 2015). Transcripts were purified using the RNA Nucleospin Clean up kit (Macherey-Nagel, Bethlehem, PA). *FF* and reporter *RLuc* constructs were co-injected at 50 ng/μL. Dual luciferase assays were performed using the Promega™ Dual-Luciferase™ Reporter (DLR™) Assay Systems with the Promega™ GloMax™ 20/20 Luminometry System (Promega, Madision, WI). 50 embryos at the mesenchyme blastula stage (24hpf) were collected in 25 μL of 1× Promega passive lysis buffer and vortexed at room temperature. The rest of the assay was performed as previously described (Stepicheva et al., 2015).

4.6. Quantification

To compare the spatial-temporal expression of miR-124 using FISH, we imaged all the embryos at the same gain with the 40× water lens on the Zeiss LSM 980 multiphoton confocal microscope and took the 30 slices at 1 μm intervals to compile a maximum intensity projection using Zen software (Carl Zeiss Incorporation, White Plains, NY). Using Zen software, we used the same parameters for adjusting the intensity of all the images.

To count the number of blastocoelar cells we used Observer Z.1 microscope (Carl Zeiss Incorporation, White Plains, NY) with a 20× air lens with a numerical aperture 0.8 and Z-stacks were taken in 1 μm intervals with 60 slices to obtain images spanning the entire embryo. Of note is that the exposure time was the same for the control compared to the experimental sets. The camera we used was Axiocam MRm 1.4 MP (Number of Pixels: 1388 × 1040, Pixel Size: 6.45 μm × 6.45 μm) (Carl Zeiss Incorporation, White Plains, NY). To count the cells, we went through the Z-stack and made sure that the FISH green fluorescence was within a region containing a nucleus counterstained with DAPI. A similar approach was used to count the pigment cells labeled with Sp1, double FISH experiments, and the number of proliferating BCs and PCs using Click-iT cell proliferation assay (Invitrogen, Waltham, MA).

4.7. Click-iT EdU assay to test cell proliferation

Reagents from the kit were diluted as instructed by the manufacturer (Invitrogen, Waltham, MA). We incubated the embryos in 10 μM EdU solution at 16hpf for 30 min at 15 °C, followed by FISH fixation (4% PFA, 1% Tween-20, 1% MOPs 1 M pH7, diluted in neutral sea water) for 1 h. These embryos are subsequently subjected to FISH with DIG and DNP-labeled RNA probes. The anti-DIG-HRP antibody was amplified with Cy3 (excitation 555 nm, orange) diluted at 1:150 in the Tyramide signal amplification (TSA) solution and were washed 6 times with MOPs buffer. The embryos were then quenched in 3% H_20_2 for 1 h at room temperature in the dark and then washed with MOPs buffer, followed by addition of anti-DNP-HRP antibody in blocking overnight at 4 °C. The anti-DNP-HRP antibody was amplified with Cy5.5 (excitation 683 nm, far-red) diluted at 1:150 in TSA solution. After the embryos were exposed to the TSA amplification steps, the embryos were washed 3 times with MOPs buffer and then once with PBST-0.5% Triton-X for 20 min at room temperature. The embryos were then washed twice with 1XPBS in 3% BSA and then the Click-iT Alexa 488 (excitation 499, green) solution was added to the embryos in the dark for 30 min at room temperature. The embryos were washed two times with 1XPBS and counterstained with DAPI. The embryos were imaged with Observer Z.1 microscope (Carl Zeiss Incorporation, White Plains, NY) with a 20× air lens with a numerical aperture 0.8 using the Axiocam MRm 1.4 MP camera for counting of BCs and PCs (Carl Zeiss Incorporation, White Plains, NY). Representative embryos were imaged on Zeiss LSM 880 scanning confocal microscope or Zeiss LSM 980 multiphoton confocal microscope (Carl Zeiss Incorporation, White Plains, NY). The maximum intensity projections of Z-stack of images were acquired with Zen software (Zeiss, White Plains, NY) and exported into Adobe Photoshop (Adobe, San Jose, CA) for further processing.

4.8. miRNA qPCR

500 embryos were collected at various time points (egg, 2 cell, 32-cell, 12hpf, 18hpf, and 24hpf). RNA was extracted from the samples using miRNeasy Mini Kit (Qiagen, Germantown, MD; Cat# 217004) and was used to make cDNA with miRCURY LNA reverse transcription Kit (Qiagen, Germantown, MD). qPCR was preformed using cbr-miR-124a miRCURY LNA miRNA PCR Assay and SPU-miR-200-3p miRCURY LNA miRNA PCR Assay (as control for normalization) (Qiagen, Germantown, MD). 10 μL total volume with a concentration of 10 ng/μL was obtained for each of the developmental stages. miR-124 levels were normalized to the miR-200 which is relatively constant throughout development (Song et al., 2012). qPCR was conducted using the QuantStudio 6 Real-Time PCR cycler system (Thermo Fisher Scientific, Waltham, MA). miR-124 levels were then normalized to the 2-cell stage using the $2^{-\Delta\Delta Ct}$ method as previously described (Sampilo et al., 2021; Stepicheva and Song, 2015).

Author contributions

K.D.K., S.S., and J.L.S. conceived the experiments. K.D.K. performed and analyzed all the experiments. M.A. and M.T. performed double fluorescence *in situ* hybridization experiments with miR-124 and *Not* or *Notch*. K.D.K and J.L.S. wrote the paper.

Funding

This work is funded from National Science Foundation Division of Integrative Organismal Systems (IOS 1553338), National Science Foundation Division of Molecular and Cellular Biosciences (MCB 2103453), and National Institutes of Health P20GM103653, National Institutes of Health (NIGMS) P20GM103446, National Institutes of Health 1S10RR027273-01, and Sigma Xi Grant-in-Aid of Research (G2018031596227966 to K.D.K.).

Declaration of competing interest

The authors declare that they have no known competing financial interests or personal relationships that could have appeared to influence the work reported in this paper.

Data availability

Data will be made available on request.

Acknowledgments

We thank Dr. David McClay (Duke University) for 1D5 antibody. We also thank the anonymous reviewers for their time and valuable feedback.

Appendix A. Supplementary data

Supplementary data to this article can be found online at https://doi.org/10.1016/j.ydbio.2023.06.017.

References

Alberti, C., Cochella, L., 2017. A framework for understanding the roles of miRNAs in animal development. Development 144, 2548–2559.
Angerer, L.M., Yaguchi, S., Angerer, R.C., Burke, R.D., 2011. The evolution of nervous system patterning: insights from sea urchin development. Development 138, 3613.
Anglicheau, D., Muthukumar, T., Suthanthiran, M., 2010. MicroRNAs: small RNAs with big effects. Transplantation 90, 105–112.
Arshinoff, B.I., Cary, G.A., Karimi, K., Foley, S., Agalakov, S., Delgado, F., Lotay, V.S., Ku, C.J., Pells, T.J., Beatman, T.R., Kim, E., Cameron, R.A., Vize, P.D., Telmer, Cheryl A., Croce, J.C., Ettensohn, C.A., Hinman, V.F., 2022. Echinobase: leveraging an extant model organism database to build a knowledgebase supporting research on the genomics and biology of echinoderms. Nucleic Acids Res. 50, D970–D979.
Baonza, A., Freeman, M., 2005. Control of cell proliferation in the Drosophila eye by Notch signaling. Dev. Cell 8, 529–539.
Bartel, D.P., 2004. MicroRNAs: genomics, biogenesis, mechanism, and function. Cell 116, 281–297.
Bartel, D.P., 2009. MicroRNAs: target recognition and regulatory functions. Cell 136, 215–233.
Bartel, D.P., 2018. Metazoan MicroRNAs. Cell 173, 20–51.
Bessodes, N., Haillot, E., Duboc, V., Rottinger, E., Lahaye, F., Lepage, T., 2012. Reciprocal signaling between the ectoderm and a mesendodermal left-right organizer directs left-right determination in the sea urchin embryo. PLoS Genet. 8, e1003121.
Bhaskaran, M., Mohan, M., 2014. MicroRNAs: history, biogenesis, and their evolving role in animal development and disease. Vet. Pathol. 51, 759–774.
Buckley, K.M., Rast, J.P., 2017. An organismal model for gene regulatory networks in the gut-associated immune response. Front. Immunol. 8, 1297.
Cai, W.L., Huang, W.D., Li, B., Chen, T.R., Li, Z.X., Zhao, C.L., Li, H.Y., Wu, Y.M., Yan, W.J., Xiao, J.R., 2018. microRNA-124 inhibits bone metastasis of breast cancer by repressing Interleukin-11. Mol. Cancer 17, 9.
Cavalieri, V., Spinelli, G., 2014. Early asymmetric cues triggering the dorsal/ventral gene regulatory network of the sea urchin embryo. Elife 3, e04664.
Chen, J.S., Pedro, M.S., Zeller, R.W., 2011. miR-124 function during Ciona intestinalis neuronal development includes extensive interaction with the Notch signaling pathway. Development 138, 4943–4953.
Croce, J.C., McClay, D.R., 2010. Dynamics of Delta/Notch signaling on endomesoderm segregation in the sea urchin embryo. Development 137, 83–91.
Duboc, V., Lapraz, F., Saudemont, A., Bessodes, N., Mekpoh, F., Haillot, E., Quirin, M., Lepage, T., 2010. Nodal and BMP2/4 pattern the mesoderm and endoderm during development of the sea urchin embryo. Development 137, 223–235.
Duboc, V., Lepage, T., 2008. A conserved role for the nodal signaling pathway in the establishment of dorso-ventral and left-right axes in deuterostomes. J. Exp. Zool. B Mol. Dev. Evol. 310, 41–53.
Ettensohn, C.A., McClay, D.R., 1988. Cell lineage conversion in the sea urchin embryo. Dev. Biol. 125, 396–409.
Ettensohn, C.A., Ruffins, S.W., 1993. Mesodermal cell interactions in the sea urchin embryo: properties of skeletogenic secondary mesenchyme cells. Development 117, 1275–1285.
Fan, P., Chen, Z., Tian, P., Liu, W., Jiao, Y., Xue, Y., Bhattacharya, A., Wu, J., Lu, M., Guo, Y., Cui, Y., Gu, W., Yue, J., 2013. miRNA biogenesis enzyme Drosha is required for vascular smooth muscle cell survival. PLoS One 8, e60888.
Floc'hlay, S., Molina, M.D., Hernandez, C., Haillot, E., Thomas-Chollier, M., Lepage, T., Thieffry, D., 2021 20. Deciphering and modelling the TGF-β signalling interplays specifying the dorsal-ventral axis of the sea urchin embryo. Development 148 (2) dev189944.
Ghafouri-Fard, S., Shoorei, H., Bahroudi, Z., Abak, A., Majidpoor, J., Taheri, M., 2021. An update on the role of miR-124 in the pathogenesis of human disorders. Biomed. Pharmacother. 135, 111198.

Gibson, A.W., Burke, R.D., 1985. The origin of pigment cells in embryos of the sea urchin Strongylocentrotus purpuratus. Dev. Biol. 107, 414–419.
Hibino, T., Loza-Coll, M., Messier, C., Majeske, A.J., Cohen, A.H., Terwilliger, D.P., Buckley, K.M., Brockton, V., Nair, S.V., Berney, K., Fugmann, S.D., Anderson, M.K., Pancer, Z., Cameron, R.A., Smith, L.C., Rast, J.P., 2006. The immune gene repertoire encoded in the purple sea urchin genome. Dev. Biol. 300, 349–365.
Ho, E.C., Buckley, K.M., Schrankel, C.S., Schuh, N.W., Hibino, T., Solek, C.M., Bae, K., Wang, G., Rast, J.P., 2017. Perturbation of gut bacteria induces a coordinated cellular immune response in the purple sea urchin larva. Immunol. Cell Biol. 95, 647.
Hou, Q., Ruan, H., Gilbert, J., Wang, G., Ma, Q., Yao, W.D., Man, H.Y., 2015. MicroRNA miR124 is required for the expression of homeostatic synaptic plasticity. Nat. Commun. 6, 10045.
Hunter, G.L., Hadjivasiliou, Z., Bonin, H., He, L., Perrimon, N., Charras, G., Baum, B., 2016. Coordinated control of Notch/Delta signalling and cell cycle progression drives lateral inhibition-mediated tissue patterning. Development 143, 2305–2310.
Joshi, I., Minter, L.M., Telfer, J., Demarest, R.M., Capobianco, A.J., Aster, J.C., Sicinski, P., Fauq, A., Golde, T.E., Osborne, B.A., 2009. Notch signaling mediates G1/S cell-cycle progression in T cells via cyclin D3 and its dependent kinases. Blood 113, 1689–1698.
Kobayashi, T., Papaioannou, G., Mirzamohammadi, F., Kozhemyakina, E., Zhang, M., Blelloch, R., Chong, M.W., 2015. Early postnatal ablation of the microRNA-processing enzyme, Drosha, causes chondrocyte death and impairs the structural integrity of the articular cartilage. Osteoarthritis Cartilage 23, 1214–1220.
Konrad, K.D., Song, J.L., 2022. miR-124 regulates Notch and NeuroD1 to mediate transition states of neuronal development. Dev. Neurobiol. 83 (1–2), 3–27. https://doi.org/10.1002/dneu.22902. PMID: 36336988.
Li, E., Materna, S.C., Davidson, E.H., 2013. New regulatory circuit controlling spatial and temporal gene expression in the sea urchin embryo oral ectoderm GRN. Dev. Biol. 382, 268–279.
Liu, L., Zhang, L., Zhao, S., Zhao, X.Y., Min, P.X., Ma, Y.D., Wang, Y.Y., Chen, Y., Tang, S.J., Zhang, Y.J., Du, J., Gu, L., 2019. Non-canonical Notch signaling regulates actin remodeling in cell migration by activating PI3K/AKT/Cdc42 pathway. Front. Pharmacol. 10, 370.
Materna, S.C., Davidson, E.H., 2012. A comprehensive analysis of Delta signaling in pre-gastrular sea urchin embryos. Dev. Biol. 364, 77–87.
Materna, S.C., Ransick, A., Li, E., Davidson, E.H., 2013. Diversification of oral and aboral mesodermal regulatory states in pregastrular sea urchin embryos. Dev. Biol. 375, 92–104.
McClay, D.R., G, W.C., Wessel, G.M., Fink, R.D., Marchase, R.B., 1983. Patterns of antigenic expression in early sea urchin development. Time, Space, Pattern Embryonic Dev. 157–169. New York: A.R. Liss.
McGeary, S.E., Lin, K.S., Shi, C.Y., Pham, T.M., Bisaria, N., Kelley, G.M., Bartel, D.P., 2019. The biochemical basis of microRNA targeting efficacy. Science 366.
Minokawa, T., 2017. Comparative studies on the skeletogenic mesenchyme of echinoids. Dev. Biol. 427, 212–218.
Nair, S.V., Del Valle, H., Gross, P.S., Terwilliger, D.P., Smith, L.C., 2005. Macroarray analysis of coelomocyte gene expression in response to LPS in the sea urchin. Identification of unexpected immune diversity in an invertebrate. Physiol. Genom. 22, 33–47.
Ohguro, Y., Takata, H., Kominami, T., 2011. Involvement of Delta and Nodal signals in the specification process of five types of secondary mesenchyme cells in embryo of the sea urchin, Hemicentrotus pulcherrimus. Dev. Growth Differ. 53, 110–123.
Perillo, M., Paganos, P., Spurrell, M., Arnone, M.I., Wessel, G.M., 2021. Methodology for whole mount and fluorescent RNA in situ hybridization in echinoderms: single, double, and beyond. In: Carroll, D.J., Stricker, S.A. (Eds.), Developmental Biology of the Sea Urchin and Other Marine Invertebrates: Methods and Protocols. Springer US, New York, NY, pp. 195–216.
Peter, I.S., Davidson, E.H., 2011. A gene regulatory network controlling the embryonic specification of endoderm. Nature 474, 635–639.
Peterson, R.E., McClay, D.R., 2005. A Fringe-modified Notch signal affects specification of mesoderm and endoderm in the sea urchin embryo. Dev. Biol. 282, 126–137.
Qadir, A.S., Woo, K.M., Ryoo, H.M., Yi, T., Song, S.U., Baek, J.H., 2014. MiR-124 inhibits myogenic differentiation of mesenchymal stem cells via targeting Dlx5. J. Cell. Biochem. 115, 1572–1581.
Range, R.C., Glenn, T.D., Miranda, E., McClay, D.R., 2008. LvNumb works synergistically with Notch signaling to specify non-skeletal mesoderm cells in the sea urchin embryo. Development 135, 2445–2454.
Ransick, A., Rast, J.P., Minokawa, T., Calestani, C., Davidson, E.H., 2002. New early zygotic regulators expressed in endomesoderm of sea urchin embryos discovered by differential array hybridization. Dev. Biol. 246, 132–147.
Revilla-i-Domingo, R., Oliveri, P., Davidson, E.H., 2007. A missing link in the sea urchin embryo gene regulatory network: hesC and the double-negative specification of micromeres. Proc. Natl. Acad. Sci. U. S. A. 104, 12383–12388.
Ruffins, S.W., Ettensohn, C.A., 1996. A fate map of the vegetal plate of the sea urchin (Lytechinus variegatus) mesenchyme blastula. Development 122, 253–263.
Sampilo, N.F., Stepicheva, N.A., Song, J.L., 2021. microRNA-31 regulates skeletogenesis by direct suppression of Eve and Wnt1. Dev. Biol. 472, 98–114.
Sampilo, N.F., Stepicheva, N.A., Zaidi, S.A.M., Wang, L., Wu, W., Wikramanayake, A., Song, J.L., 2018. Inhibition of microRNA suppression of Dishevelled results in Wnt pathway-associated developmental defects in sea urchin. Development 145.
Sethi, A.J., Angerer, R.C., Angerer, L.M., 2014. Multicolor labeling in developmental gene regulatory network analysis. Methods Mol. Biol. 1128, 249–262.
Sharma, T., Ettensohn, C.A., 2011. Regulative deployment of the skeletogenic gene regulatory network during sea urchin development. Development 138, 2581–2590.
Sherwood, D.R., McClay, D.R., 1999. LvNotch signaling mediates secondary mesenchyme specification in the sea urchin embryo. Development 126, 1703–1713.
Smith, L.C., Ghosh, J., Buckley, K.M., Clow, L.A., Dheilly, N.M., Haug, T., Henson, J.H., Li, C., Lun, C.M., Majeske, A.J., Matranga, V., Nair, S.V., Rast, J.P., Raftos, D.A., Roth, M., Sacchi, S., Schrankel, C.S., Stensvag, K., 2010. Echinoderm immunity. Adv. Exp. Med. Biol. 708, 260–301.
Solek, C.M., Oliveri, P., Loza-Coll, M., Schrankel, C.S., Ho, E.C., Wang, G., Rast, J.P., 2013. An ancient role for Gata-1/2/3 and Scl transcription factor homologs in the development of immunocytes. Dev. Biol. 382, 280–292.
Song, J.L., Stoeckius, M., Maaskola, J., Friedlander, M.R., Stepicheva, N., Juliano, C., Lebedeva, S., Thompson, W., Rajewsky, N., Wessel, G.M., 2012. Select microRNAs are essential for early development in the sea urchin. Dev. Biol. 362, 104–113.
Stepicheva, N., Nigam, P.A., Siddam, A.D., Peng, C.F., Song, J.L., 2015. microRNAs regulate beta-catenin of the Wnt signaling pathway in early sea urchin development. Dev. Biol. 402, 127–141.
Stepicheva, N.A., Song, J.L., 2014. High throughput microinjections of sea urchin zygotes. J. Vis. Exp., e50841
Stepicheva, N.A., Song, J.L., 2015. microRNA-31 modulates skeletal patterning in the sea urchin embryo. Development 142, 3769–3780.
Suzuki, H., Yaguchi, S., 2018. Transforming growth factor-β signal regulates gut bending in the sea urchin embryo. Dev. Growth Differ. 60, 216–225.
Sweet, H.C., Gehring, M., Ettensohn, C.A., 2002. LvDelta is a mesoderm-inducing signal in the sea urchin embryo and can endow blastomeres with organizer-like properties. Development 129, 1945–1955.
Tamboline, C.R., Burke, R.D., 1992. Secondary mesenchyme of the sea urchin embryo: ontogeny of blastocoelar cells. J. Exp. Zool. 262, 51–60.
Weitzel, H.E., Illies, M.R., Byrum, C.A., Xu, R., Wikramanayake, A.H., Ettensohn, C.A., 2004. Differential stability of beta-catenin along the animal-vegetal axis of the sea urchin embryo mediated by dishevelled. Development 131, 2947–2956.
Yang, F., Qi, J., 2020. miR-430a regulates the development of left-right asymmetry by targeting sqt in the teleost. Gene 144628. Gene. 30;745:144628.